

## DIRECT NUMERICAL SIMULATION STUDY OF WATER DROPLETS FREEZING ON A HORIZONTAL PLATE

Pham Duy Binh<sup>1,2</sup>, Vu Van Truong<sup>1,\*</sup>, Nguyen Thi Viet Lien<sup>2</sup>,  
Nguyen Tien Cuong<sup>1</sup>, Nguyen Dinh Hoe<sup>1,2</sup>, Nguyen Tuan Vinh<sup>1,2</sup>, Vu Van Hung<sup>3</sup>

<sup>1</sup>Faculty of Vehicle and Energy Engineering, Phenikaa University, Ha Noi, Viet Nam

<sup>2</sup>Graduate University of Science and Technology, Vietnam Academy of Science and Technology,  
18 Hoang Quoc Viet, Cau Giay, Ha Noi, Viet Nam

<sup>3</sup>School of Transportation Engineering, Hanoi University of Science and Technology,  
01 Dai Co Viet, Hai Ba Trung, Hanoi, Viet Nam

\*Emails: [truong.vuvan@phenikaa-uni.edu.vn](mailto:truong.vuvan@phenikaa-uni.edu.vn)

Received: 29 August 2020; Accepted for publication: 3 March 2021

**Abstract.** There are many experiments on solidification (i.e. freezing) of water droplets on the cold plate but the numerical investigation of its freezing process is very little. So, to provide an understanding of that, we present a numerical method and its results to describe the solidification process of water droplets on a cold plate at different wetting angles ( $\phi_0$ ) in the range of 30° - 155°. The Navier-Stokes and energy equations are used and solved by an axisymmetric front-tracking/finite difference technique. The distinct phases are separated by the interfaces represented by connected elements. So, there is a three-junction point among three phases: solid, liquid, and gas. The water droplets are assumed as a spherical cap and placed on the cold plate which is kept at a subfreezing temperature. At the end of solidification, we obtain a small protrusion shape at the top of the frozen water droplet and its height is also higher than that of the initial water droplet. That is explained by the increase in volume upon freezing because of the difference in densities of water and ice. The frozen water droplets are also compared with the corresponding experimental ones reported in the literature.

**Keywords:** front-tracking method, freezing process, water droplet, wetting angle.

**Classification numbers:** 4.10.4, 5.4.4.

### 1. INTRODUCTION

The solidification of water droplets can find in nature and industrial processes such as the freezing water droplets on wind turbines, aircraft, air conditioning, fridge and any cooling types of equipment [1 - 4]. It may cause serious hazards as reducing the performance of machines or decreasing their lifetime. Providing energy to remove the ice on the surface is one of the good ideas but it seems to be expensive and influences the performance of machines, too. Using chemical compounds is another choice but it may cause bad effects on the environment. Therefore, deep understandings of the freezing process would be a significant task for researchers to find the solution to avoid the damage as well as enhance the efficiency of

machines. The spreading and solidification process of water drop was investigated at different contact angles (*i.e.* wetting angles) ( $\phi_0$ ) by Huang *et al.* [5] as well as by Pan *et al.* [6] in the range of  $76^\circ - 155^\circ$  and  $77^\circ - 145^\circ$ , respectively. In the same work [6], Pan *et al.* also studied the solidification of water droplet on an inclined surface ( $\varphi = 30^\circ$ ). The freezing process of a water droplet was monitored on different cold concave surfaces with radii ( $R$ ) in the range of 10 mm – 25 mm and  $R = \infty$  [7] as well as on spherical surfaces with radii ( $R$ ) ranging from 15 mm to 30 mm. In this study, we only consider the solidification of a water droplet on a cold flat surface.

Numerically, Shetabivash *et al.* [9] presented a multi-level-set approach to simulate the solidification process of water droplet on a flat surface. In another research, Vahab *et al.* [10] used the level-set approach and the moment of fluid method to consider the solidification of a water droplet on a substrate in order to apply to aircraft icing. Ajaev and Davis [11] applied the boundary integral method [12] to simulate the solidification process of droplet. However, these researches did not consider the solidification of a water droplet at different wetting angles ( $\phi_0$ ). To fill this gap, we represent a front-tracking method [13] to numerically simulate the freezing process of water droplets on a horizontal plate.

## 2. NUMERICAL MODEL AND METHOD

The problem? is described in .

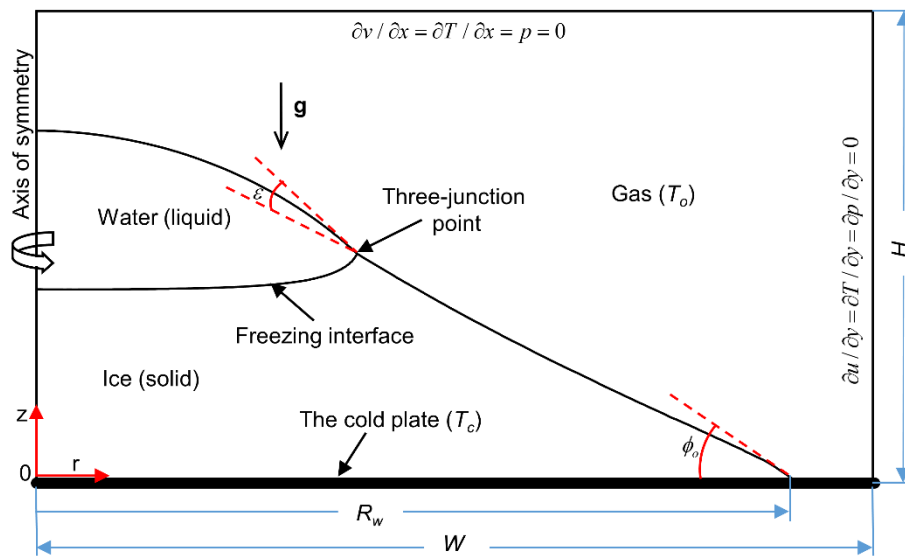


Figure 1. Computational domain of the freezing process of a water droplet on a cold plate at growth angle ( $\varepsilon$ ) and wetting angle ( $\phi_0$ ).

The shape of the water droplet is assumed to have a spherical cap. Because of the symmetry of the droplet, we only simulated a half of the droplet which is placed on a cold plate ( $T_c$ ) in a computational domain  $W \times H$ . The interfaces separate three phases: solid, liquid, and gas. Thus, there are three interfaces, namely solid-liquid, solid-gas and liquid-gas. Accordingly, there is the presence of a three-junction point. We use the Navier-Stokes and energy equations to solve the problem, and the front-tracking method [14] is used to represent the phase boundaries. The liquid and gas in this study are supposed to be incompressible, immiscible and Newtonian. In

each phase, density  $\rho$ , viscosity  $\mu$ , heat capacity  $C_p$  and thermal conductivity  $k$  are constant, the Navier-Stokes and continuity equations are:

$$\frac{\partial(\rho\mathbf{u})}{\partial t} + \nabla\rho\mathbf{u}\mathbf{u} = -\nabla p + \nabla\left[\mu\left(\nabla\mathbf{u} + \nabla\mathbf{u}^T\right)\right] + \int_f \sigma\kappa\delta(\mathbf{x} - \mathbf{x}_f)\mathbf{n}_f dS + \rho(\mathbf{f} + \mathbf{g}) \quad (1)$$

$$\nabla\cdot\mathbf{u} = \frac{1}{L_h}\left(\frac{1}{\rho_s} - \frac{1}{\rho_l}\right)\int_f \delta(\mathbf{x} - \mathbf{x}_f)\dot{q}dS \quad (2)$$

here,  $\mathbf{u}$  is the velocity vector,  $p$  is the pressure,  $\sigma$  and  $\kappa$  are the interfacial tension coefficient and twice mean curvature, respectively. The Dirac delta function is denoted by  $\delta$ ,  $\mathbf{x}$  is the position vector, subscript  $f$  expresses the interface,  $\mathbf{n}$  is the unit normal vector, force  $\mathbf{f}$  is used to apply the non-slip condition on the solid interface [15 - 18],  $\mathbf{g}$  is the gravitational acceleration,  $L_h$  is the latent heat of fusion,  $\dot{q}$  is thermal flux at the solid-liquid interface, subscripts  $s$  and  $l$  represent solid and liquid, respectively.

With  $T$  - temperature,  $k$  - thermal conductivity,  $C_p$  - heat capacity, the energy equation is:

$$\frac{\partial(\rho C_p T)}{\partial t} + \nabla(\rho C_p T\mathbf{u}) = \nabla(k\nabla T) + \int_f \dot{q}\delta(\mathbf{x} - \mathbf{x}_f)dS \quad (3)$$

The dimensionless parameters are important in our study. They give us a general vision about their impacts. The dimensionless parameters used are:

$$Pr = \frac{C_{pl}\mu_l}{k_l}, St = \frac{C_{pl}(T_m - T_c)}{L_h}, Bo = \frac{\rho_l g R^2}{\sigma}, We = \frac{\rho_l U_c^2 R}{\sigma} = \frac{k_l^2}{\rho_l \sigma R C_l^2} \quad (4)$$

$$\theta_0 = \frac{T_0 - T_c}{T_m - T_c}, \rho_{sl} = \frac{\rho_s}{\rho_l}, \rho_{gl} = \frac{\rho_g}{\rho_l}, \mu_{gl} = \frac{\mu_g}{\mu_l}, \mu_{sl} = \frac{\mu_s}{\mu_l} \quad (5)$$

$$k_{sl} = \frac{k_s}{k_l}, k_{gl} = \frac{k_g}{k_l}, C_{psl} = \frac{C_{ps}}{C_{pl}}, C_{pgl} = \frac{C_{pg}}{C_{pl}} \quad (6)$$

here,  $Pr$ ,  $St$ ,  $Bo$ ,  $We$  are Prandtl number, Stefan number, Bond number, Weber number,  $\theta_0$  - initial dimensionless temperature,  $\rho_{sl}$ ,  $\rho_{gl}$  - density ratios,  $\mu_{sl}$ ,  $\mu_{gl}$  - viscosity ratios,  $k_{sl}$ ,  $k_{gl}$  - thermal conductivity ratios,  $C_{psl}$ ,  $C_{pgl}$  - heat capacity ratios. The non-dimensional time is  $\tau = t/\tau_c$ . Here,  $\tau_c = \rho_l C_{pl} R^2 / k_l$  is reference time,  $R = [3V_o / (4\pi)]^{1/3}$  - equivalent radius,  $V_o$  - initial volume of the water droplet.

In this study, the front-tracking technique with the finite difference scheme, previously presented in some works [13, 19], is applied, where the interfaces include the points  $\mathbf{x}_f$  connected to each other, and each point moves with the velocity  $\mathbf{V}_n$  which is interpolated from the nearest grid points:

$$\mathbf{x}_f^{n+1} = \mathbf{x}_f^n + \mathbf{V}_n \Delta t \quad (7)$$

with the time evolution,  $t$  and  $t + \Delta t$  correspond to steps  $n$  and  $n + 1$ . Thanks to the points  $\mathbf{x}_f$ , we can compute the interfacial tension forces acting on the interfaces and hence build the indicator functions to identify the properties of the phase. To determine the distinct phases, we use two indicator functions  $I_1$  and  $I_2$  reconstructed from the positions of the interfaces. The value of each indicator function is 1 in a fluid and 0 in another one. The subscripts  $s$ ,  $l$ , and  $g$  are for solid,

liquid, and gas, respectively. Thus, the properties of the phases at every position in the computational domain are given as [20, 21]:

$$\rho = [\rho_s I_1 + \rho_l (1 - I_1)] I_2 + \rho_g (1 - I_2) \quad (8)$$

$$\mu = [\mu_s I_1 + \mu_l (1 - I_1)] I_2 + \mu_g (1 - I_2) \quad (9)$$

More details about our method can be found in some previous works [13, 19].

### 3. RESULTS AND DISCUSSION

#### 3.1. Water droplet at a wetting angle $\phi_o = 78^\circ$

Figure 2 shows the time evolution of the freezing water droplet at a wetting angle  $\phi_o = 78^\circ$  placed on a cold plate. With  $R = 1.41$  mm ( $D_i = 2.82$  mm [6]), the parameters include  $Pr = 7$ ,  $St = 0.1$ ,  $Bo = 0.27$ ,  $We = 0.005$ ,  $\theta_o = 1$ ,  $\rho_{sl} = 0.9$ ,  $\rho_{gl} = 0.05$ ,  $\mu_{sl} = 1$ ,  $\mu_{gl} = 0.05$ ,  $k_{sl} = 4$ ,  $k_{gl} = 0.05$ ,  $C_{psl} = 0.5$ , and  $C_{pgl} = 0.2$ . At time  $\tau = 0$  (Figure 2a), the water droplet is assumed to have a spherical cap. The whole droplet is in the liquid state and its density has got the highest value. At  $\tau = 0.26$  (Figure 2b), the distinct regions (solid and liquid) are established with the appearance of a freezing interface between them. The density difference between ice and water can be seen in Figure 2b, where the density in the region under the freezing interface is smaller than that above

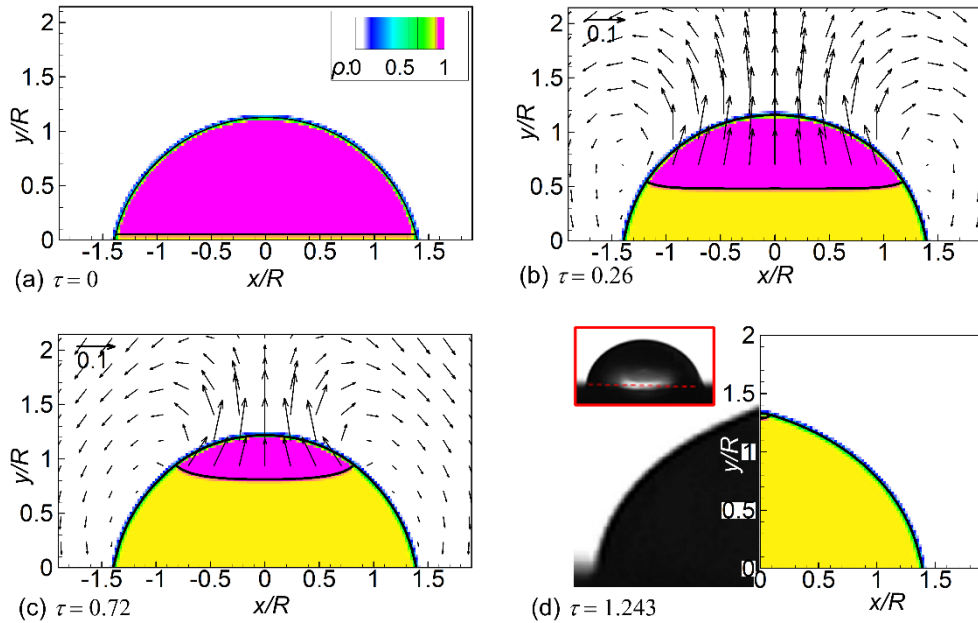


Figure 2. The time evolution of ice during the freezing process of a water droplet at  $\phi_o = 78^\circ$ . (a)-(c) correspond to  $\tau = 0$ ,  $\tau = 0.26$  and  $\tau = 0.72$  with the density field ( $\rho$ ), and the velocity vectors normalized by  $U_c = R/t_c$ . (d) Comparison in the shape of the frozen droplet between the numerical simulation (right) and the experiment of Pan *et al.* [6] (left). In (d), the inset in the top-left corner shows the initial water droplet on the cold plate in the experiment.

the freezing interface, which reflects a property of water (the density of ice is smaller than that of water). Besides, a velocity field is presented in Figure 2b. Over time, at  $\tau = 0.72$  (Figure 2c), the region of the solid state of the water droplet is increased, this is in contrast to the decrease of the region of the fluid state of the water droplet. Similarly, the distinct regions of the water droplet, density field, velocity field can be seen in Figure 2c. Finally, at  $\tau = 1.243$  (Figure 2d), the solidification process of the water droplet is almost finished. The protrusion of the frozen water droplet's top appeared; this feature can be explained by the volume expansion. We compare our study with the experiment of Pan *et al.* [6] at a wetting angle  $\phi_o = 78^\circ$ . In Figure 2d, our study is in the right frame and the experiment of Pan *et al.* [6] is in the left frame. As reported by Pan *et al.* [6], the water droplet was initially a part of a sphere (see the inset in the top-left corner of the left frame in Figure 2d) because of surface tension acting on the water-gas interface, and it became a frozen water droplet with an apex at the droplet top as shown in the left frame (Figure 2d). As can be seen in Figure 2d, our numerical model agrees well with the experiment of Pan *et al.* [6].

### 3.2. Water droplet at a wetting angle $\phi_o = 124^\circ$

Figure 3 illustrates the freezing process of the water droplet that possesses a wetting angle  $\phi_o = 124^\circ$  with  $Pr = 7.5$ ,  $St = 0.1$ ,  $Bo = 0.18$ ,  $We = 0.005$ ,  $\theta_o = 1$ ,  $\rho_{sl} = 0.9$ ,  $\rho_{gl} = 0.05$ ,  $\mu_{sl} = 1$ ,  $\mu_{gl} = 0.05$ ,  $k_{sl} = 4$ ,  $k_{gl} = 0.05$ ,  $C_{psl} = 0.5$ , and  $C_{pgl} = 0.2$  (initial volume  $V_o = 6 \mu\text{l}$  [5]). Similar to the previous case, we assume that the initial water droplet has a spherical cap. The cold plate is kept at subfreezing temperature  $T_c$ . At time  $\tau = 0$  (Figure 3a), the normalized temperature  $\theta$  has the highest value excepting the region near the cold plate. At  $\tau = 0.5$  (Figure 3b), the interface

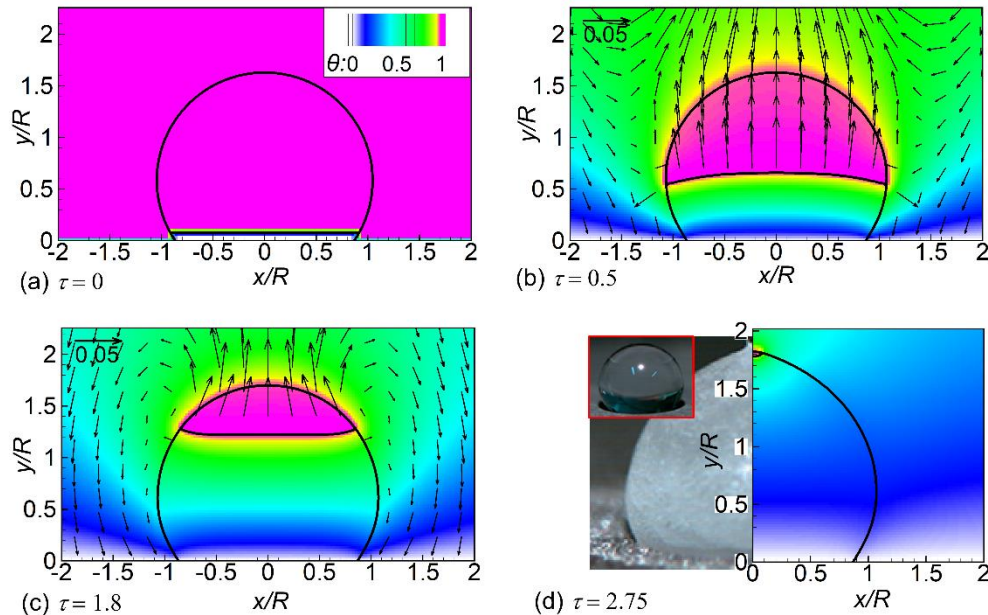


Figure 3. The time evolution of the water droplet with  $\phi_o = 124^\circ$  freezing on the plate. (a)-(c) correspond to  $\tau = 0$ ,  $\tau = 0.5$  and  $\tau = 2.74$  with the temperature field ( $\theta$ ) and the velocity vectors normalized by  $U_c = R/t_c$ . (d) Comparison between the numerical simulation (right) and the experiment of Huang et al [5] (left). In (d), the inset in the top-left corner shows the initial water droplet on the cold plate in the experiment.

between ice and water moves from the bottom to the top of the water droplet. Along with the movement of the interface, over time, the normalized temperature around the water droplet decreases gradually because of the cooling effects of the cold plate. At  $\tau = 1.8$  (Figure 3c), the region having the subfreezing temperature extends from the cold plate to the top of the domain. Finally, at  $\tau = 2.74$  (Figure 3d), the solidification process of the water droplet is almost complete. Similar to the previous case, we can see a shape like a horn on top of the water droplet. This feature is induced by the volume expansion. This case is compared with the experiment of Huang *et al.* [5] at a wetting angle  $\phi_o = 124^\circ$ . In Figure 3d, our study is in the right frame and the experiment of Huang *et al.* [5] is in the left one. As reported by Huang and co-workers [5], at the beginning of the freezing process, the water droplet has a spherical cap (see the inset in the top-left corner of the left frame in Figure 3d) due to the surface tension force. The droplet became a frozen one with an apex at the droplet top at the end of freezing, as shown in the left frame (Figure 3d). Figure 3d confirms that the computed frozen droplet and that reported in Huang *et al.* [5] match very well.

### 3.3. Water droplet at a wetting angle $\phi_o = 155^\circ$

Figure 4 describes the solidification process with the time evolution of the freezing interface of the water droplet at a wetting angle  $\phi_o = 155^\circ$ . The parameters include  $Pr = 7.5$ ,  $St = 0.1$ ,  $Bo = 0.18$ ,  $We = 0.005$ ,  $\theta_o = 1$ ,  $\rho_{sl} = 0.9$ ,  $\rho_{gl} = 0.05$ ,  $\mu_{sl} = 1$ ,  $\mu_{gl} = 0.05$ ,  $k_{sl} = 4$ ,  $k_{gl} = 0.05$ ,  $C_{psl} = 0.5$ , and  $C_{pgl} = 0.2$  (initial volume  $V_o = 6\mu\text{l}$  [5]). Firstly, at  $\tau = 0$  (Figure 4a), the initial droplet shape with normalized temperature  $\theta$  is presented. The whole domain excepting the region near the cold plate has the highest temperature. Secondly, at  $\tau = 0.72$  (Figure 4b) the freezing

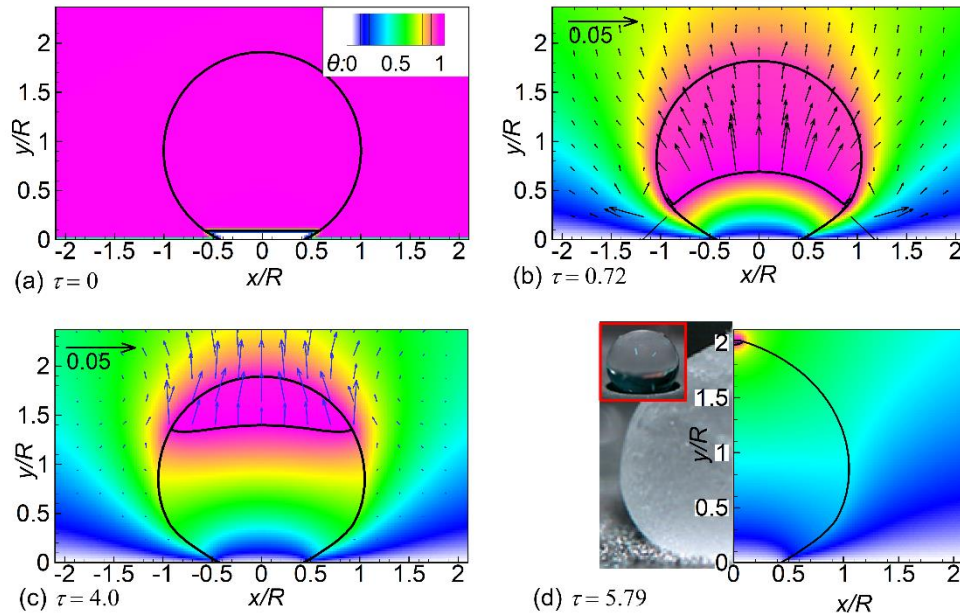


Figure 4. The time evolution of the ice layer of the water droplet with  $\phi_o = 155^\circ$ . (a)-(c) correspond to  $\tau = 0$ ,  $\tau = 0.72$  and  $\tau = 5.79$  with the temperature field ( $\theta$ ), the velocity vectors normalized by  $U_c = R/t_c$ . (d) Comparison between the numerical simulation (right) and the experiment Huang *et al* [5] (left). In (d), the inset in the top-left corner shows the initial water droplet on a cold plate in the experiment.

interface of the droplet moves from the bottom to the top. Along with the movement of the freezing interface, from the bottom of the drop to its top, the normalized temperature has got low to high temperatures, the solidification happens at the location where it's temperature below the freezing temperature of water. Then, at  $\tau = 4.0$  (Figure 4c), the normalized temperature expands from the bottom to the top of the domain, more and more area of the droplet is frozen. Hence, the liquid region of the droplet is decreased, this is in contrast to the increase in the solid region when time proceeds. Finally, at  $\tau = 5.79$ , as we can see from Figure 4d, the solidification of the water droplet is almost finished. A shape of the frozen droplet with a horn is formed. Similar to the previous case, we compare this case (at a wetting angle  $\phi_o = 155^\circ$ ) to the experiment of Huang et al. [5]. In Figure 4d, our study is shown in the right frame and the left one is the experiment of Huang et al. [5]. Like the previous cases (Figure 2d and Figure 3d), the water droplet with a spherical cap at the beginning of the freezing process (see the inset in the top-left corner of the left frame of Figure 4d) [5] became a frozen one with a conical top surface at the end of freezing (the left frame of Figure 4d). There is not much difference between the simulated and experimental droplets as shown in Figure 4d.

### 3.4. Variations of freezing water droplets on a cold plate at different wetting angles

Experimentally, Satunkin [22] studied the solidification of molten silicon and germanium droplets at a wetting angle of about  $33^\circ$ . For water droplets, Huang *et al.* [5] conducted experiments on their solidification at wetting angles in the range of  $76^\circ - 154.9^\circ$ . In the work of Pan *et al.* [6], the wetting angle of water droplets was varied in the range of  $77^\circ - 145^\circ$ . It is found that the wetting angle of a liquid droplet on a cold plate studied in the aforementioned works is in the range of  $30^\circ - 155^\circ$ . To our knowledge, no further investigation on a water droplet

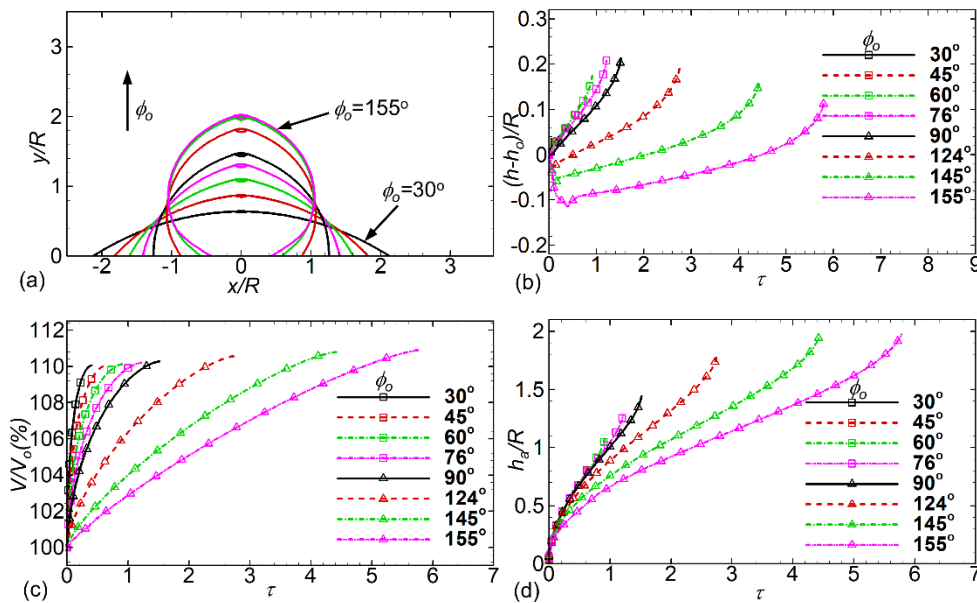


Figure 5. Variations of freezing water droplets at different wetting angles by evolution time  $\tau$ . (a) The shapes of the ice droplets after complete solidification process. (b) The evolution height of the droplets before and after solidification process,  $h$  is the height of the droplet,  $h_o$  is the initial height of the droplet. (c) Proportion of the volume and the initial volume of the droplets with time. (d) The average freezing interface heights of the droplets  $h_a$  with time.

at a wetting angle out of this range has been conducted so far. Accordingly, basing on our literature survey, we vary the wetting angle in the range of  $30^\circ - 155^\circ$  to investigate the solidification process of water droplets.

Figure 5 illustrates the effects of the wetting angles  $\phi_o$  in the range of  $30^\circ - 155^\circ$  on the freezing process of a water droplet with the parameters  $Pr = 7.5$ ,  $St = 0.1$ ,  $Bo = 0.18$ ,  $We = 0.005$ ,  $\theta_o = 1$ ,  $\rho_{sl} = 0.9$ ,  $\rho_{gl} = 0.05$ ,  $\mu_{sl} = 1$ ,  $\mu_{gl} = 0.05$ ,  $k_{sl} = 4$ ,  $k_{gl} = 0.05$ ,  $C_{psl} = 0.5$ , and  $C_{pgl} = 0.2$  (initial volume  $V_o = 6 \mu\text{l}$  [5]). Figure 5a shows the shapes of the droplets after the complete solidification process, where the height of the ice droplets increases with increasing the wetting angle. We can see the increasing heights of the droplets in Figure 5b. After finishing the freezing process, the evolution height,  $h - h_o$ , of the droplet increases with increasing the wetting angle in the range of  $30^\circ - 90^\circ$ . In contrast, further increasing the wetting angle from  $90^\circ$  to  $155^\circ$  causes the evolution height of the droplet to be decreased. Interestingly, the evolution heights of the droplets at wetting angles in the range of  $90^\circ - 155^\circ$  all have got the negative values during the initial stage of the freezing process. This can be explained by the effect of the gravitational acceleration. As mentioned, the initial droplets were assumed to be spherical and have an initial volume  $V_o$ . The droplets having a great height and a small area of contact with the cold plate are more affected by gravity. Therefore, the height of the water droplet is pulled down during the initial stage of the freezing process, resulting in the negative value of  $h - h_o$  as shown in Figure 5b. Figure 5c presents the temporal variation of the ratio, in terms of %, of the volume  $V$  of the droplet to its initial volume  $V_o$ . It is clear that the volume of the droplet increases as the freezing process proceeds. After complete solidification process, the volume rises about 10 % as compared to the initial volume because of the volume expansion of the water drop upon freezing. In addition, the solidification time increases with an increase in the wetting angle in the range of  $30^\circ - 155^\circ$ . This can be explained by the contact area of the droplet with the cold plate. The larger the contact area of the droplet, the faster the solidification. Figure 5d shows the variation with respect to time of the mean value of the freezing interface height of the droplet. The solidification process finished with the maximum average interface height at a wetting angle  $\phi_o = 155^\circ$ . It indicates that decreasing the wetting angle will enhance the freezing process.

#### 4. CONCLUSIONS

The numerical model was presented to simulate the freezing of water droplets on a cold plate under the influence of the wetting angles  $\phi_o$ . We consider the temporal evolution of the freezing process and compare with the experiments of Pan *et al.* [6] ( $\phi_o = 78^\circ$ ) and Huang *et al.* [5] ( $\phi_o = 124^\circ$  and  $\phi_o = 155^\circ$ ). The results of the numerical simulations agree well with the experiments. The shape of the droplet after complete solidification process, the evolution height of the droplet, the percentage of the droplet volume compared to its initial volume, and the average freezing interface height were presented. After ending the solidification process, we can see the top of the droplets like a horn and that can be explained by the volume expansion of the water droplet upon freezing.

**Acknowledgements.** This research is funded by Vietnam National Foundation for Science and Technology Development (NAFOSTED) under grant number 107.03-2019.307.

**CRedit authorship contribution statement.** Pham Duy Binh: Methodology, Investigation, Formal analysis, Writing original-draft. Vu Van Truong: Methodology, Supervision, Reviewing and Editing. Nguyen Thi Viet Lien: Supervision. All authors: Visualization, Formal analysis.

**Declaration of competing interest.** The authors declare that they have no known competing financial interests or personal relationships that could have appeared to influence the work reported in this paper.

## REFERENCES

1. Andersson L. O., Golander C. G., and Persson S. - Ice adhesion to rubber materials, *Journal of Adhesion Science and Technology* **8** (1994) 117-132.
2. Cebeci T. and Kafyeke F. - Aircraft Icing, *Annu. Rev. Fluid. Mech.* **35** (2003) 11-21.
3. Dalili N., Edrissy A., and Carriveau R. - A review of surface engineering issues critical to wind turbine performance, *Renewable and Sustainable Energy Reviews* **13** (2009) 428-438.
4. Lian W. and Xuan Y. - Experimental investigation on a novel aero-engine nose cone anti-icing system, *Applied Thermal Engineering* **121** (2017) 1011-1021.
5. Huang L., Liu Z., Liu Y., Gou Y., and Wang L. - Effect of contact angle on water droplet freezing process on a cold flat surface, *Experimental Thermal and Fluid Science* **40** (2012) 74-80.
6. Pan Y., Shi K., Duan X., and Naterer G. F. - Experimental investigation of water droplet impact and freezing on micropatterned stainless steel surfaces with varying wettabilities, *International Journal of Heat and Mass Transfer* **129** (2019) 953-964.
7. Zhang H., Jin Z., Jiao M., and Yang Z. - Experimental investigation of the impact and freezing processes of a water droplet on different cold concave surfaces, *International Journal of Thermal Sciences* **132** (2018) 498-508.
8. Ju J., Jin Z., Zhang H., Yang Z., and Zhang J. - The impact and freezing processes of a water droplet on different cold spherical surfaces, *Experimental Thermal and Fluid Science* **96** (2018) 430-440.
9. Shetabivash H., Dolatabadi A., and Paraschivoiu M. - A multiple level-set approach for modelling containerless freezing process, *Journal of Computational Physics* **415** (2020) 109527.
10. Vahab M., Pei C., Hussaini M. Y., Sussman M., and Lian Y. - An Adaptive Coupled Level Set and Moment-of-Fluid Method for Simulating Droplet Impact and Solidification on Solid Surfaces with Application to Aircraft Icing, 54th AIAA Aerospace Sciences Meeting, American Institute of Aeronautics and Astronautics, San Diego, California, USA.
11. Ajaev V. S. and Davis S. H. - Boundary-integral simulations of containerless solidification, *Journal of Computational Physics* **187** (2003) 492-503.
12. Wardle L. - *An Introduction to the Boundary Element Method*, North-Holland Mathematics Studies, Elsevier, pp. 525-551.
13. Tryggvason G., Bunner B., Esmaeeli A., Juric D., Al-Rawahi N., Tauber W., Han J., Nas S., and Jan Y. J. - A Front-Tracking Method for the Computations of Multiphase Flow, *Journal of Computational Physics* **169** (2001) 708-759.
14. Vu T. V., Tryggvason G., Homma S., and Wells J. C. - Numerical investigations of drop solidification on a cold plate in the presence of volume change, *Int. J. Multiphase Flow* **76** (2015) 73-85.

15. Vu T. V., Truong A. V., Hoang N. T. B., and Tran D. K. - Numerical investigations of solidification around a circular cylinder under forced convection, *J. Mech. Sci. Technol.* **30** (2016) 5019-5028.
16. Vu T. V. and Wells J. C. - Numerical simulations of solidification around two tandemly-arranged circular cylinders under forced convection, *Int. J. Multiphase Flow* **89** (2017) 331-344.
17. Duy V. N. and Vu T. V. - A numerical study of a liquid drop solidifying on a vertical cold wall, *Int. J. Heat Mass Transfer* **127** (2018) 302-312.
18. Vu T. V. - Deformation and breakup of a pendant drop with solidification, *Int. J. Heat Mass Transfer* **122** (2018) 341-353.
19. Vu T. V., Tryggvason G., Homma S., Wells J. C., and Takakura H. - A Front-Tracking Method for Three-Phase Computations of Solidification with Volume Change, *Journal of Chemical Engineering of Japan* **46** (2013) 726-731.
20. Vu T. V. - Fully resolved simulations of drop solidification under forced convection, *Int. J. Heat Mass Transfer* **122** (2018) 252-263.
21. Vu T. V., Vu T. V., and Bui D. T. - Numerical study of deformation and breakup of a multi-core compound droplet in simple shear flow, *Int. J. Heat Mass Transfer* **131** (2019) 1083-1094.
22. Satunkin G. A. - Determination of growth angles, wetting angles, interfacial tensions and capillary constant values of melts, *J. Cryst. Growth* **255** (2003) 170-189.